THE JOURNAL OF PHYSICAL CHEMISTRY Letters

pubs.acs.org/JPCL Letter

Finite Temperature Dynamical Density Matrix Renormalization Group for Spectroscopy in Frequency Domain

Tong Jiang, Weitang Li, Jiajun Ren,* and Zhigang Shuai*

Cite This: J. Phys. Chem. Lett. 2020, 11, 3761−3768 Read Online

ACCESS | Metrics & More | Article Recommendations | Supporting Information

ABSTRACT: We present a novel methodology through casting the dynamical density matrix renormalization group (DDMRG) into the matrix product state (MPS) formulation to calculate the spectroscopy at finite temperature for molecular aggregates. The frequency domain algorithm can avoid the time evolution accumulation of error and is naturally suitable for parallelization, in addition to facile graphic processing unit (GPU) acceleration. The high accuracy is demonstrated by simulating the optical spectra of vibronic model systems ranging from an exactly solvable dimer model to a more complex real-world perylene bisimide (PBI) J-aggregate. The relationship between the 0−0 emission strength and the exciton thermal coherent length is discussed for linearly stacked aggregates. The computing performance largely boosted by GPU demonstrates that DDMRG emerges as a promising method to study dynamical properties for complex systems.

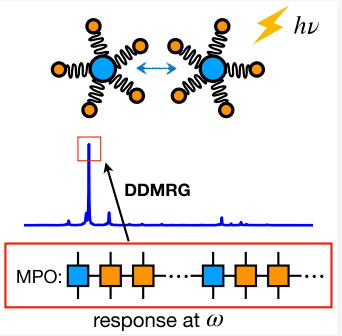

Density matrix renormalization group (DMRG) was initially developed for the electronic structure of strongly correlated systems, especially for one-dimensional lattice models,[1,2] and immediately it has been applied to quantum chemistry from semiempirical Hamiltonian to ab initio calculation.[3−7] Recently, the time-dependent (TD) formulation of DMRG, called TD-DMRG,[8−11] has also been used to calculate the real-time dynamics and spectroscopy of electron-vibration coupled systems, including the linear optical spectroscopy,[12] exciton dissociation,[13] ultrafast internal conversion,[14,15] and singlet fission.[16,17] Combined with the purification method,[18−20] the thermal equilibrium properties or temperature-dependent dynamical properties could also be calculated by directly time-evolving the density matrix.[12] In a very short time, TD-DMRG has emerged as an efficient and effective quantum dynamics method for a complex system.

Nevertheless, the accuracy of TD-DMRG is restricted by the maximum accessible time,[21,22] as a result of the quick growth of entanglement during the time evolution. It has been reported that great care must be taken when investigating the transport properties because the long time evolution would sometimes give a seemingly converged but actually unreliable diffusion coefficient.[23] A similar problem will emerge when calculating the spectrum with high resolution because of the Fourier relationship between time and frequency. However, the frequency domain DMRG methods[11,24−31] can provide a different perspective to avoid the time evolution problem. The original Lanczos-DMRG[24] and the newly proposed Chebyshev matrix product state (CheMPS)[30] are both modified moments expansion methods with the advantage of producing the entire spectrum by one batch of calculation. However, the prerequisite of these methods is that the vectors in the Krylov space should be orthogonal to each other, which would be violated due to the truncation error in DMRG, in addition to the round-off error. In that case, it is hard to obtain a high-resolution spectra, although it has been shown that carrying out the costly reorthonormalization could partly relieve this problem.[32,33] On another side, correction vector (CV)-DMRG was developed by Ramasesha and Shuai et al. for both linear and nonlinear responses,[25,26] which targets one frequency at one time calculation. Based on CV-DMRG, a variational algorithm, termed as dynamical DMRG (DDMRG), was suggested by Jeckelmann,[28] which was shown to have improved accuracy. All of these methods were initially developed for response properties at zero temperature. Only recently have the Lanczos-DMRG and CheMPS been extended to finite temperature.[34,35]

Here, we propose an algorithm to extend DDMRG to finite temperature and reformulate it in the framework of matrix product state to overcome several drawbacks of the original DDMRG algorithm. We will demonstrate that such an approach can serve as an accurate and reliable route to calculate the linear response function at finite temperature for molecular aggregates and could be largely accelerated with the state-of-the-art algorithm and hardware.

Received: March 22, 2020
Accepted: April 22, 2020
Published: April 22, 2020

https://dx.doi.org/10.1021/acs.jpclett.0c00905
J. Phys. Chem. Lett. 2020, 11, 3761−3768

In DMRG, the wave function and operator could be represented by the matrix product state (MPS) and the matrix product operator (MPO),[36,37]

$$|\Psi\rangle = \sum_{\{a\},\{\sigma\}} A^{\sigma_1}_{a_1} A^{\sigma_2}_{a_1 a_2} \cdots A^{\sigma_N}_{a_{N-1}} |\sigma_1 \sigma_2 \cdots \sigma_N\rangle \tag{1}$$

$$\hat{O} = \sum_{\{w\},\{\sigma\},\{\sigma'\}} W^{\sigma_1',\sigma_1}_{w_1} W^{\sigma_2',\sigma_2}_{w_1 w_2} \cdots W^{\sigma_N',\sigma_N}_{w_{N-1}} |\sigma_1' \sigma_2' \cdots \sigma_N'\rangle\langle\sigma_N \sigma_{N-1} \cdots \sigma_1| \tag{2}$$

where σ_i is the local basis with dimension d. One good feature of DMRG is that the accuracy is solely determined by the dimension of A^{σ_i}, named (virtual) bond dimension M, and thus could be systematically improved.

According to the linear response theory, the spectral function of optical spectroscopy is

$$S(\omega) = -\frac{1}{\pi} \lim_{\eta \to 0^+} \mathrm{Im}(\chi^{(1)}(\omega) - \chi^{(2)}(\omega)) \tag{3}$$

$$\chi^{(1)}(\omega) = \mathrm{Tr}\left(\hat{\mu} \frac{1}{\omega - \mathcal{L} + i\eta} \hat{\mu} \rho_\beta\right) \tag{4}$$

$$\chi^{(2)}(\omega) = \mathrm{Tr}\left(\hat{\mu} \frac{1}{\omega + \mathcal{L} + i\eta} \hat{\mu} \rho_\beta\right) \tag{5}$$

where $\mathcal{L} = [\hat{H}_0, \cdot]$ is the Liouville superoperator and $\hat{\mu}$ is the dipole operator. For $\omega > 0$, the two terms $\chi^{(1)}(\omega)$ and $\chi^{(2)}(\omega)$ physically represent the stimulated absorption and stimulated emission, respectively. Between them, $\chi^{(2)}(\omega)$ could be omitted safely for absorption spectrum when the energy gap between the ground state and the excited state is much larger than the energy scale of temperature, which is usually the case for the electronic spectroscopy in the ultraviolet−visible region at room temperature. But for the infrared absorption, it is necessary to calculate both the two terms, which have a relation $\chi^{(1)}(-\omega)^* = -\chi^{(2)}(\omega)$.

We define the correction vector $C(\omega)$ at finite temperature as

$$C(\omega) = \frac{1}{(\omega - \mathcal{L} + i\eta)} \hat{\mu} \rho_\beta^{1/2} \tag{6}$$

Here, $C(\omega)$ is an MPO and $\rho_\beta^{1/2} = e^{-\beta \hat{H}_0/2}/\sqrt{Z(\beta)}$ ($Z(\beta) = \mathbf{Tr}(e^{-\beta H_0})$), which could be obtained by integrating the imaginary time Schrödinger eq (eq 7) from $\tau = 0$ to $\tau = \beta/2$. Since eq 7 is not unitary, $\rho(\tau)$ is normalized with condition $\langle\langle \rho(\tau)|\rho(\tau)\rangle\rangle = \mathrm{Tr}(\rho^\dagger(\tau)\rho(\tau)) = 1$ after each step of evolution.

$$-\frac{\partial}{\partial \tau} \rho(\tau) = \hat{H}_0 \rho(\tau) \tag{7}$$

The initial state $\rho(0)$ at infinitely high temperature is a locally maximally entangled state $\rho(0) = \prod_i \sum_{\sigma_i} \frac{1}{\sqrt{d}} |\sigma_i\rangle\langle\sigma_i|$, which is easily represented by an MPO with $M = 1$.[12,36] In this work, we adopt the time-dependent variational principle based variable mean field algorithm (TDVP-VMF) for imaginary time evolution.[38] The time step is adaptively chosen by the Dormand−Princes 5/4 Runge−Kutta algorithm. To avoid coping with a non-Hermitian matrix, the imaginary part of the correction vector, $X(\omega)$, fulfills the following real symmetric and positive definite linear equation:

$$((\omega - \mathcal{L})^2 + \eta^2) X(\omega) = -\eta \hat{\mu} \rho_\beta^{1/2} \tag{8}$$

Analogous to the zero temperature DDMRG, a Hylleraas-like functional is defined as

$$L[X(\omega)] = \mathrm{Tr}\{X^\dagger((\omega - \mathcal{L})^2 + \eta^2)X + 2\eta X^\dagger \hat{\mu} \rho_\beta^{1/2}\} \tag{9}$$

Since the global minimum of L lies exactly at the point where $X(\omega)$ satisfies eq 8, eq 8 could be solved by minimizing $L[X(\omega)]$. The main advantage of DDMRG compared to CV-DMRG is that the spectral function could be obtained directly from the minimal value of $L[X(\omega)]$,

$$S(\omega) = -L[X(\omega)]_{\min}/\pi\eta \tag{10}$$

Therefore, the error of $S(\omega)$ is $O(\varepsilon^2)$ if $X(\omega)$ has error $O(\varepsilon)$ and $S(\omega)$ is a lower bound of the exact value.[28]

In the original DDMRG algorithm, $X(\omega)$ and the ground state wave function share the same set of renormalized basis using the state-average method.[28] We improve this approximation by expressing $X(\omega)$ and $\rho_\beta^{1/2}$ with two independent MPOs as the newly proposed DDMRG^{++}.[11] $X(\omega)$ can be obtained by solving the uncoupled linear equations $\partial L/\partial A^{\sigma_i}_{a_{i-1}a_i} = 0$ (eq 11) locally by sweeps following the philosophy of DMRG.[36]

$$\frac{\partial L}{\partial A^{\sigma_i}} = \mathrm{Tr}\left\{ X^\dagger[(\omega - \hat{H}_0)^2 + \eta^2] \frac{\partial X}{\partial A^{\sigma_i}} + 2X^\dagger(\omega - \hat{H}_0) \frac{\partial X}{\partial A^{\sigma_i}} \hat{H}_0 + X^\dagger \frac{\partial X}{\partial A^{\sigma_i}} \hat{H}_0^2 + \eta \rho_\beta^{1/2} \hat{\mu} \frac{\partial X}{\partial A^{\sigma_i}} \right\} = 0 \tag{11}$$

The linear equation is illustrated graphically in Figure 1. The second improvement we use here is that the high order moments such as $\mathrm{Tr}\left\{X(\omega)|(\omega - \hat{H}_0)^2|\frac{\partial}{\partial A^{\sigma_i}} X(\omega)\right\}$ is exactly calculated since $\hat{H}_0$ is represented by an exact MPO rather than approximated in the renormalized space $\hat{P}\hat{H}_0\hat{P}$, where

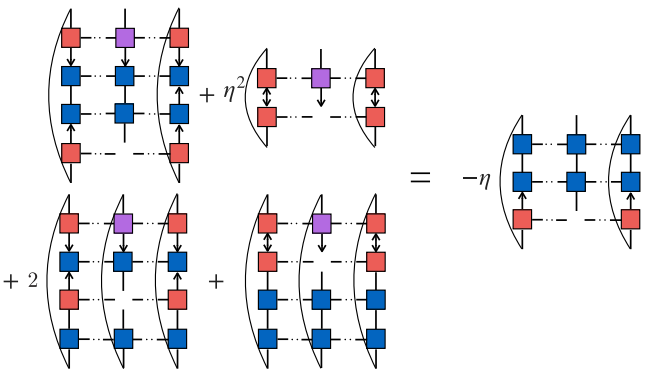

Figure 1. Linear equation $\partial L/\partial A^{\sigma_i}_{a_{i-1}a_i} = 0$ (eq 11) to optimize the local site $A^{\sigma_i}_{a_{i-1}a_i}$(in purple) at finite temperature. The operators $(\omega - \hat{H}_0)$, $\hat{H}_0$, $\hat{\mu}$, and $\rho_\beta^{1/2}$ are shown in blue and the correction vector $X(\omega)$ is shown in red.

https://dx.doi.org/10.1021/acs.jpclett.0c00905
J. Phys. Chem. Lett. 2020, 11, 3761−3768

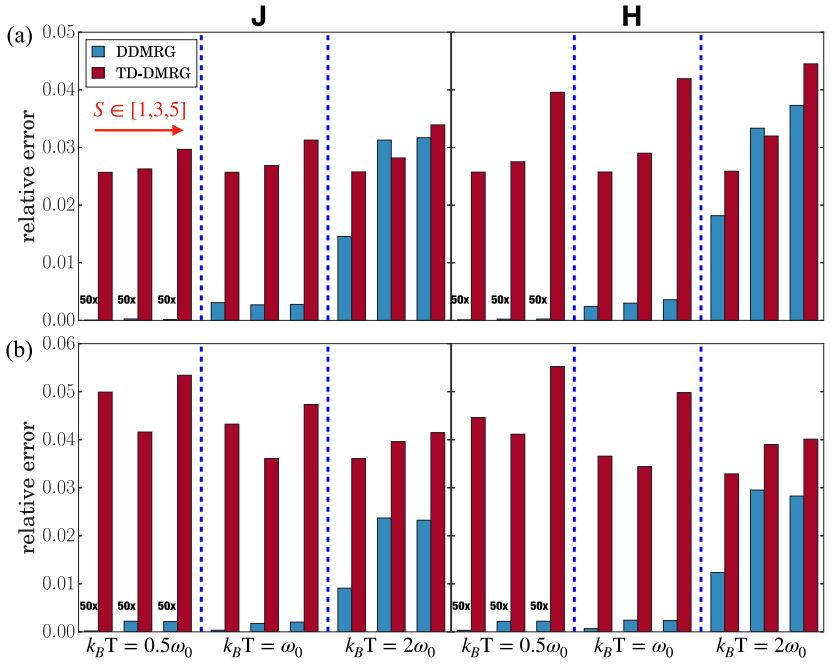

Figure 2. Relative error of (a) absorption and (b) emission spectra for J- and H- aggregates with different Huang−Rhys factor ($S \in [1.0, 3.0, 5.0]$) across different temperature ($k_BT \in [0.5\omega_0, \omega_0, 2\omega_0]$). Note the error of DDMRG at $k_BT = 0.5\omega_0$ is magnified 50 times to make it clearly visible.

$P = \sum_{\sigma_i, a_{i-1}a_i} \left| \frac{\partial}{\partial A^{\sigma_i}_{a_{i-1}a_i}} X(\omega) \right\rangle \left\langle \frac{\partial}{\partial A^{\sigma_i}_{a_{i-1}a_i}} X(\omega) \right|$.[11,28] We also present the MPS formulation of DDMRG at zero temperature in the Supporting Information.

Now we apply DDMRG to investigate the finite temperature optical spectra for molecular aggregate, as represented by the Frenkel−Holstein exciton model,

$$\hat{H} = \sum_i \varepsilon_i a_i^\dagger a_i + \sum_{ij} J_{ij} a_i^\dagger a_j + \sum_{in} \omega_{in} b_{in}^\dagger b_{in} + \sum_{in} \omega_{in} g_{in} a_i^\dagger a_i (b_{in}^\dagger + b_{in}) \quad (12)$$

where ε_i is the adiabatic excitation energy of the ith molecule, J_{ij} is the intersite electronic coupling between the ith and jth molecules, ω_{in} and g_{in} refer to the harmonic frequency and dimensionless electron-vibrational coupling strength of the nth normal mode of the ith molecule. The absorption (emission) cross section is obtained by multiplying the frequency dependence ω (ω^3) as a prefactor separately. For simplicity, we neglect the aggregate geometry factor and assume that the orientations of all local transition dipole moments are the same.

We first examine the accuracy of DDMRG by comparing it with TD-DMRG on a toy dimer model with one vibrational mode of frequency ω_0 for each molecule with up to 16 vibrational quanta. Benchmarks on the absorption and emission spectra are carried out in comparison with exact diagonalization (ED). The exciton-vibrational coupling varies by adjusting the Huang−Rhys factor ($S = g^2 \in [1.0, 3.0, 5.0]$). J- and H-type aggregates are investigated by setting the excitonic coupling to be $-\omega_0$ and ω_0, respectively. The relative error is defined as

$$\text{relative error}_{\text{method}} = \frac{\sum_{\{\omega_i\}} |\sigma_{\text{method}}(\omega_i) - \sigma_{\text{exact}}(\omega_i)|}{\sum_{\{\omega_i\}} \sigma_{\text{exact}}(\omega_i)} \quad (13)$$

where $\{\omega_i\}$ groups the discrete frequency points and $\sigma(\omega_i)$ is the corresponding line strength. In the TD-DMRG calculation, we employ the projector splitting evolution scheme[10,38] with time step $dt = 0.01\omega_0^{-1}$ to propagate 10 000 steps. The same bond dimension $M = 120$ and Lorentzian broadening $\eta = 0.1\omega_0$ are used in both TD-DMRG and DDMRG. The thermal equilibrium density matrices at different temperatures are obtained by imaginary time evolution with the bond dimension $M = 32$.

Figure 2 shows that both TD-DMRG and DDMRG are accurate enough with the relative error less than 6%. DDMRG is remarkably accurate especially at low temperature ($k_BT \in [0.5\omega_0, \omega_0]$). At $k_BT = 2\omega_0$, the accuracy of DDMRG deteriorates but is still a little bit better than TD-DMRG. Inspecting $X(\omega)$ expanded on the eigenstates,

$$X(\omega) = \sum_{m,n} \frac{e^{-\beta E_m/2}}{\sqrt{Z(\beta)}} \frac{-\eta \langle n|\hat{\mu}|m\rangle}{(\omega - E_n + E_m)^2 + \eta^2} |n\rangle\langle m| \quad (14)$$

the loss of accuracy with temperature of DDMRG could be qualitatively explained by the fact that, at relatively low temperature, $X(\omega)$ only contains a small set of transition pairs $|n\rangle\langle m|$ with large coefficients and thus is easy to be compressed as an MPO with a small bond dimension M. While at higher temperature, the set of transition pairs becomes larger and the compression becomes harder. Therefore, DDMRG is more suitable for problems in which the vibrations have frequencies larger than the energy scale of the temperature.

We further look into the regime $k_BT \leq \omega_0$, which is usually the case for the intramolecular vibrations at room temperature. We study the disorder-free systems composed of linearly arranged N chromophores with negative nearest-neighbor-only coupling $J_0 = -2.5\omega_0$. The Huang−Rhys factor of each vibration is $S = 1$. The n-particle approximation approach has been widely used to investigate the spectral signatures of molecular aggregates,[39−43] and as a compromise between the accuracy and computational cost, the 2-particle approximation

https://dx.doi.org/10.1021/acs.jpclett.0c00905
J. Phys. Chem. Lett. 2020, 11, 3761−3768

(2-PA) is the most popular one. We use DDMRG and 2-PA to calculate the temperature-dependent 0−0 emission I^{0-0} of the open boundary systems of different sizes and a 50-site system with periodic boundary condition in Figure 3a. The bond

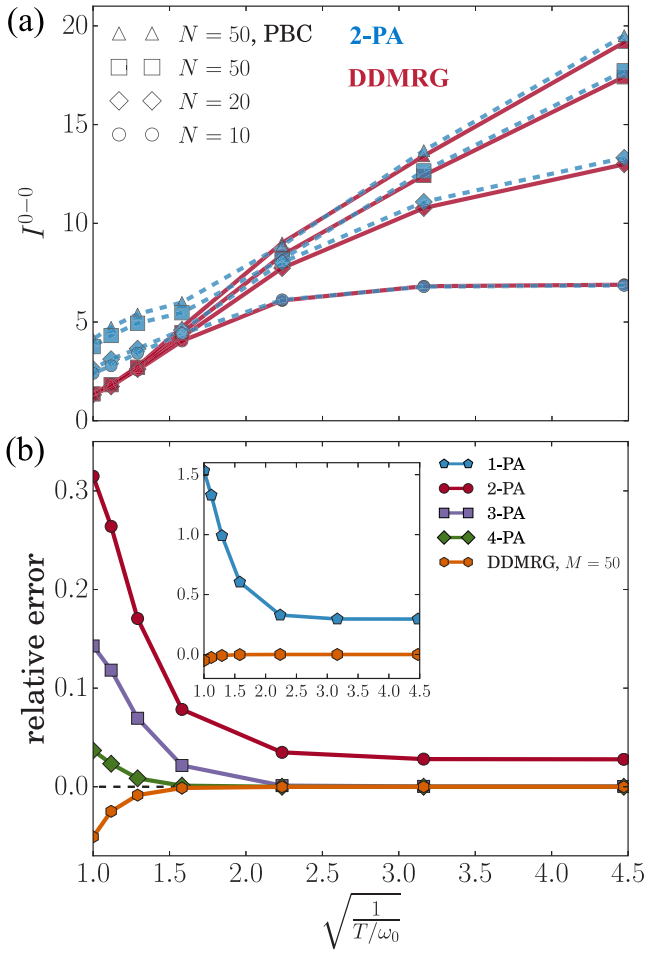

Figure 3. (a) 0−0 emission strength I^{0-0} as a function of $T^{-1/2}$ when $J_0 = -2.5\omega_0$ (A linear relationship with $T^{-1/2}$ is predicted by strong excitonic coupling perturbation theory[41]). Lines with △ are the results of a 50-site system with periodic boundary condition (M = 120), and the others are with open boundary condition (M = 100). (b) Relative error of 0−0 emission strength I^{0-0} of a 5-site system using n-particle approximation and DDMRG.

dimensions used when doing the imaginary time evolution are 64 for the 50-site system and 32 for smaller systems. The prefactor of the frequency index is omitted here to focus on the dimensionless strength alone. 2-PA agrees well with DDMRG at low temperature and exhibits evident overestimation at high temperature. To account for this, we study a 5-site system whose Hamiltonian can be treated by up to 5-PA, which is equal to ED. The relative errors by different levels of approximations are presented in Figure 3b. At high temperature, 2-PA exhibits an apparent overestimation, which is approximately 30% when $k_BT = \omega_0$. The overestimation can be reduced by including the higher-particle states, which is only feasible for small systems. DDMRG achieves comparable accuracy as the 4-PA with only M = 50. In addition, because of its variational feature, the results of DDMRG are always the lower bound of the exact values. The inset of Figure 3b shows that the result of the simplest 1-PA is much worse than the others and is not even qualitatively reliable in this 5-site system. For more details, the whole spectra obtained from different methods at $k_BT = 0.05\omega_0$ and $k_BT = \omega_0$ are shown in Figure S3. It is also worth mentioning that since n-particle approximation is a truncated configuration interaction method, it is not size-consistent and thus is expected to perform worse for larger systems, as observed in Figure 3a. For completeness, we also compare DDMRG and 2-PA at the intermediate excitonic coupling regime $J_0 = -0.25\omega_0$ and the weak excitonic coupling regime $J_0 = -0.025\omega_0$ in the Supporting Information. A similar trend has been found that DDMRG is more accurate than 2-PA at high temperature.

As shown in Figure 3a, with the decrease of temperature, I^{0-0} initially rises and subsequently levels off because of the boundary effect, and at high temperature, I^{0-0} is only related to the temperature but not to the system size as a result of the exciton−phonon interaction induced localization. Therefore, Spano and co-workers proposed to use I^{0-0} to characterize the number of coherent molecules at a specific temperature called the temperature-dependent thermal coherence size, which is important to the phenomena of superradiance observed in the molecular aggregates.[39,41] Since the information on exciton coherent length L_ρ could be obtained from the reduced density matrix $\rho_S = \mathrm{Tr}_B(\rho_\beta)$ by tracing out the vibrational degrees of freedom, we could investigate the relation between I^{0-0} and L_ρ directly. We adopt the widely used definition of exciton coherent length when characterizing the polaron size in the biological antenna complexes and organic molecular crystals:[44−46]

$$L_\rho = \frac{\left(\sum_{ij}^{N} |\rho_{S,ij}|\right)^2}{N\sum_{ij}^{N} |\rho_{S,ij}|^2} \tag{15}$$

which measures the variance of ρ_S. Figure 4 shows that the temperature dependence of I^{0-0} and L_ρ are almost parallel to

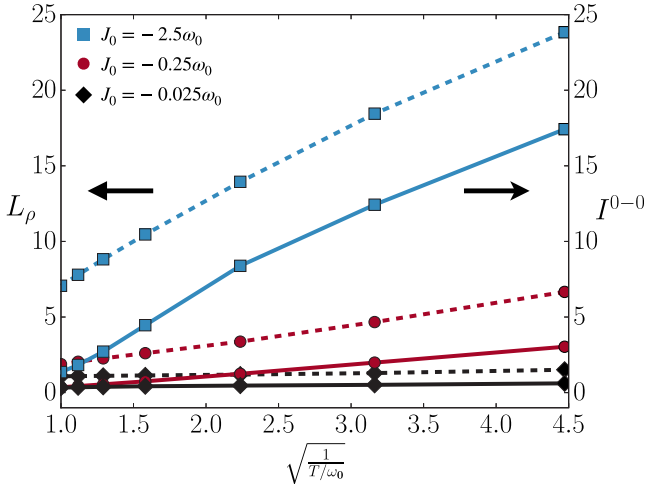

Figure 4. Temperature dependence of the exciton coherent length L_ρ and 0−0 emission strength I^{0-0} for open boundary 50-site models with different excitonic couplings.

each other in a wide range of excitonic coupling J_0, indicating a nearly linear relationship between the 0−0 emission strength and the thermal coherent length in the one-dimensional J-aggregates, which is in accordance with the results calculated by Toyozawa ansatz.[44]

https://dx.doi.org/10.1021/acs.jpclett.0c00905
J. Phys. Chem. Lett. 2020, 11, 3761−3768

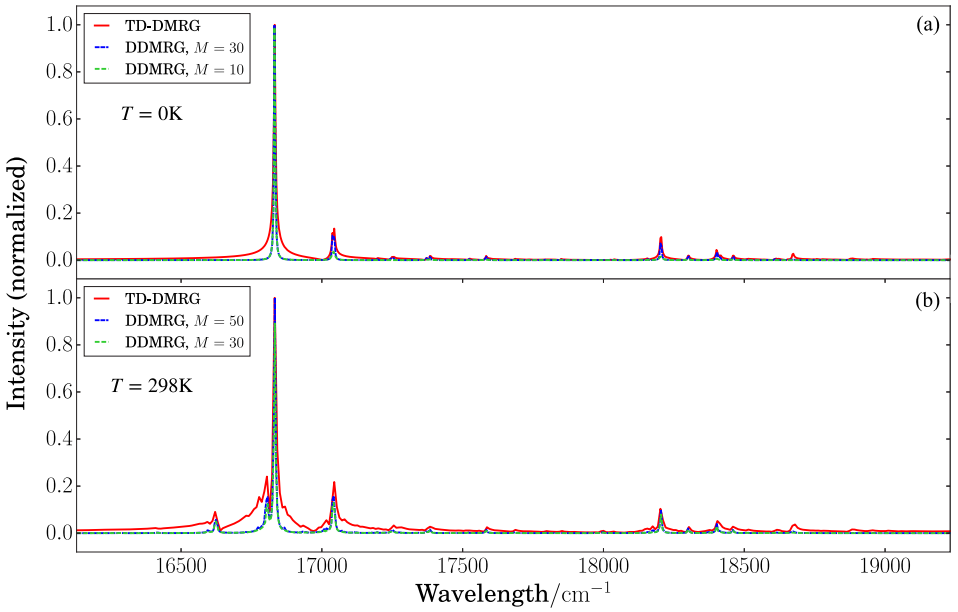

Figure 5. Absorption spectrum calculated by DDMRG and TD-DMRG (a) at 0 K and (b) at 298 K. For DDMRG, the Lorentzian broadening width is $\eta = 2$ cm^{-1}. The result of TD-DMRG is from ref 12.

We further apply DDMRG to simulate the absorption spectrum of a perylene bisimide (PBI) derivative, which has become the prototypical molecular aggregates for testing methodologies in quantum dynamics. Accurate calculations at zero temperature on the PBI chain using multiconfiguration time-dependent Hartree (MCTDH) were performed by Kühn et al.,[47,48] followed by the TD-DMRG calculation with comparable accuracy at zero temperature[12,15] and finite temperature.[12] We adopt the same model here and each molecule has ten modes with frequency from 206 to 1628 cm^{-1}.[12,15,48] Figure 5 shows that the absorption spectrum of a PBI dimer calculated by DDMRG with $M = 10(30)$ at 0 K and $M = 30(50)$ at 298 K. The results of TD-DMRG[12] with $M = 42$ at 0 K and $M = 120$ at 298 K are also plotted for comparison. Though the bond dimension is smaller, DDMRG obtains a higher resolution and more smooth spectrum than TD-DMRG, especially at finite temperature. One of the reasons is that the frequencies of intramolecular vibrations of PBI are larger than the energy scale of room temperature which is favored by DDMRG, as shown in Figure 2. Second, the resolution of the spectrum could be systematically improved by increasing the number of frequency points in DDMRG. The $\Delta\omega$ between the neighboring frequency points in DDMRG calculation is 3.3 cm^{-1}. For TD-DMRG to achieve this kind of resolution, the total evolution time is at least 10 ps, which is pretty difficult if not impossible not only in terms of accuracy but also in computational cost.

DDMRG is generally considered to be computationally expensive since many frequency points have to be calculated. However, it is perfectly scalable because each of them is independent and thus could be easily parallelized on the modern supercomputer with hundreds and thousands central processing unit (CPU) cores. Besides this trivial parallelization, the graphical processing unit (GPU) has shown its great potential in accelerating the heavy tensor contraction in DMRG.[38] We focus on the latter below and adopt a CPU-GPU heterogeneous parallelization strategy in which GPU is responsible for the tensor contraction shown in eq 11 and Figure 1 and CPU is responsible for the matrix decomposition. A calculation of 50-site Holstein model with $M = 50$ is timed by the CPU-only scheme (1 core) and by the GPU-accelerated scheme. Figures 6a,b present the time cost of each frequency at $k_BT = 0$ and $k_BT = \omega_0$. At $T = 0$, CPU-GPU heterogeneous computation is able to speed up the calculation 5 times on average and 7 times for the most time-consuming point. Better still, the acceleration at finite temperature is more remarkable with 51 times on average and 63 times for the most time-consuming point. Notably, the time cost is evidently different for different frequencies. The calculation of the resonant frequency tends to be more difficult because of the larger condition number of eq 11, requiring more steps of iteration to converge.[49] In this CPU-GPU heterogeneous calculation, the imaginary time evolution with $M = 64$ takes about 20% of the total computational time. Although the acceleration for different systems and bond dimensions shall be different, such a test case is able to demonstrate that the algorithm of DDMRG could be largely accelerated by the CPU-GPU heterogeneous parallelization.

To conclude, for the first time we generalize the dynamical density matrix renormalization group from zero temperature formalism to finite temperature formalism. The new algorithm with matrix product states/operators is more accurate in representing the correction vector and calculating the high-order moments of operators. The superiority of the frequency domain DDMRG over the time domain approach has been demonstrated by simulating the optical spectroscopy of vibronic models ranging from the simple dimer model to the real-world PBI molecular aggregate. The near-linear relationship between the thermal equilibrium exciton coherent length and 0−0 emission strength of the one-dimensional J-aggregates is verified by this highly accurate method. Moreover, the significant acceleration after adopting CPU-GPU heterogeneous parallelization strategy makes DDMRG more promising for large scale systems. We highlight the important features of DDMRG: (i) The resolution and accuracy of the spectrum could be systematically improved: more smooth spectrum is obtained by calculating more frequency points and the variational formulation guarantees the convergence for the

https://dx.doi.org/10.1021/acs.jpclett.0c00905
J. Phys. Chem. Lett. 2020, 11, 3761−3768

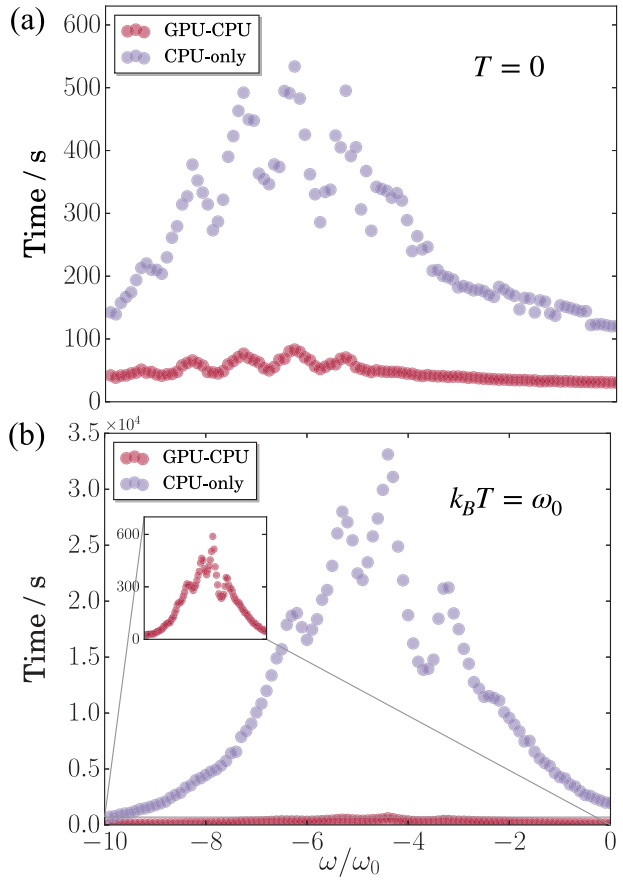

Figure 6. Time cost of a 50-site Holstein model at (a) $T = 0$ and (b) $k_BT = \omega_0$. Conditions: the local basis $p = 4$; the nearest-neighbor coupling $J_0 = -2.5\omega_0$; the Huang−Rhys factor $S = 1$; the Lorentzian broadening width $\eta = 0.1\omega_0$. The platforms are Intel Xeon CPU E5-2680 v4 @ 2.40 GHz for CPU only calculation and Intel Xeon Gold 5115 CPU @ 2.40 GHz with NVIDIA Tesla V100-PCIE-32GB for CPU-GPU heterogeneous calculations.

response intensity by merely increasing the bond dimension. (ii) It allows calculations of an arbitrary window in the frequency domain, e.g., the charge mobility can be obtained by calculating the response at $\omega = 0$ with Green−Kubo formula.[50] (iii) The algorithm is perfectly scalable on the modern distributed supercomputer.

Finally, we make some comments on the time domain approach TD-DMRG. TD-DMRG is a numerically exact and robust method suitable for ultrafast dynamics and is irreplaceable when real-time information is necessary. But like all the other quantum dynamics methods in the time domain, TD-DMRG is still hard to do accurate long-time propagation due to the enhanced entanglement as time propagation goes. The frequency domain DDMRG can naturally avoid such a problem and provides a reliable and accurate routine to compute the dynamical properties.

■ ASSOCIATED CONTENT

Supporting Information

The Supporting Information is available free of charge at https://pubs.acs.org/doi/10.1021/acs.jpclett.0c00905.

Matrix product state formulation of DDMRG at zero temperature; spectral data of the n-particle approximation (including emission strength plots and emission spectra) (PDF)

■ AUTHOR INFORMATION

Corresponding Authors

Jiajun Ren − *MOE Key Laboratory of Organic OptoElectronics and Molecular Engineering, Department of Chemistry, Tsinghua University, Beijing 100084, People's Republic of China;* orcid.org/0000-0002-1508-4943; Email: renjj@mail.tsinghua.edu.cn

Zhigang Shuai − *MOE Key Laboratory of Organic OptoElectronics and Molecular Engineering, Department of Chemistry, Tsinghua University, Beijing 100084, People's Republic of China;* orcid.org/0000-0003-3867-2331; Email: zgshuai@tsinghua.edu.cn

Authors

Tong Jiang − *MOE Key Laboratory of Organic OptoElectronics and Molecular Engineering, Department of Chemistry, Tsinghua University, Beijing 100084, People's Republic of China;* orcid.org/0000-0002-5907-4886

Weitang Li − *MOE Key Laboratory of Organic OptoElectronics and Molecular Engineering, Department of Chemistry, Tsinghua University, Beijing 100084, People's Republic of China*

Complete contact information is available at: https://pubs.acs.org/10.1021/acs.jpclett.0c00905

Notes

The authors declare no competing financial interest.

■ ACKNOWLEDGMENTS

This work is supported by the National Natural Science Foundation of China SCELMA (Science CEnter for Luminescence from Molecular Aggregates) project (grant No. 21788102) and the Ministry of Science and Technology of China (grant No. 2017YFA0204501). J.R. is also supported by the Shuimu Tsinghua Scholar Program.

■ REFERENCES

(1) White, S. R. Density matrix formulation for quantum renormalization groups. *Phys. Rev. Lett.* **1992**, *69*, 2863.

(2) White, S. R. Density-matrix algorithms for quantum renormalization groups. *Phys. Rev. B: Condens. Matter Mater. Phys.* **1993**, *48*, 10345.

(3) Shuai, Z.; Bredas, J.-L.; Pati, S. K.; Ramasesha, S. Quantum confinement effects on the ordering of the lowest-lying excited states in conjugated polymers. *Proc. SPIE* **1997**, *3145*, 293−302.

(4) Yaron, D.; Moore, E. E.; Shuai, Z.; Brédas, J. Comparison of density matrix renormalization group calculations with electron-hole models of exciton binding in conjugated polymers. *J. Chem. Phys.* **1998**, *108*, 7451−7458.

(5) Fano, G.; Ortolani, F.; Ziosi, L. The density matrix renormalization group method: Application to the PPP model of a cyclic polyene chain. *J. Chem. Phys.* **1998**, *108*, 9246−9252.

(6) White, S. R.; Martin, R. L. Ab initio quantum chemistry using the density matrix renormalization group. *J. Chem. Phys.* **1999**, *110*, 4127−4130.

(7) Chan, G. K.-L.; Head-Gordon, M. Highly correlated calculations with a polynomial cost algorithm: A study of the density matrix renormalization group. *J. Chem. Phys.* **2002**, *116*, 4462−4476.

(8) Vidal, G. Efficient simulation of one-dimensional quantum many-body systems. *Phys. Rev. Lett.* **2004**, *93*, 040502.

(9) White, S. R.; Feiguin, A. E. Real-time evolution using the density matrix renormalization group. *Phys. Rev. Lett.* **2004**, *93*, 076401.
(10) Haegeman, J.; Lubich, C.; Oseledets, I.; Vandereycken, B.; Verstraete, F. Unifying time evolution and optimization with matrix product states. *Phys. Rev. B: Condens. Matter Mater. Phys.* **2016**, *94*, 165116.
(11) Ronca, E.; Li, Z.; Jimenez-Hoyos, C. A.; Chan, G. K.-L. Time-step targeting time-dependent and dynamical density matrix renormalization group algorithms with ab initio Hamiltonians. *J. Chem. Theory Comput.* **2017**, *13*, 5560−5571.
(12) Ren, J.; Shuai, Z.; Chan, G. K. Time-Dependent Density Matrix Renormalization Group Algorithms for Nearly Exact Absorption and Fluorescence Spectra of Molecular Aggregates at Both Zero and Finite Temperature. *J. Chem. Theory Comput.* **2018**, *14*, 5027−5039.
(13) Yao, Y.; Sun, K.-W.; Luo, Z.; Ma, H. Full quantum dynamics simulation of a realistic molecular system using the adaptive time-dependent density matrix renormalization group method. *J. Phys. Chem. Lett.* **2018**, *9*, 413−419.
(14) Greene, S. M.; Batista, V. S. Tensor-train split-operator fourier transform (tt-soft) method: Multidimensional nonadiabatic quantum dynamics. *J. Chem. Theory Comput.* **2017**, *13*, 4034−4042.
(15) Baiardi, A.; Reiher, M. Large-Scale Quantum Dynamics with Matrix Product States. *J. Chem. Theory Comput.* **2019**, *15*, 3481−3498.
(16) Schröder, F. A.; Turban, D. H.; Musser, A. J.; Hine, N. D.; Chin, A. W. Tensor network simulation of multi-environmental open quantum dynamics via machine learning and entanglement renormalisation. *Nat. Commun.* **2019**, *10*, 1062.
(17) Xie, X.; Liu, Y.; Yao, Y.; Schollwöck, U.; Liu, C.; Ma, H. Time-dependent density matrix renormalization group quantum dynamics for realistic chemical systems. *J. Chem. Phys.* **2019**, *151*, 224101.
(18) Verstraete, F.; Garcia-Ripoll, J. J.; Cirac, J. I. Matrix product density operators: simulation of finite-temperature and dissipative systems. *Phys. Rev. Lett.* **2004**, *93*, 207204.
(19) Zwolak, M.; Vidal, G. Mixed-state dynamics in one-dimensional quantum lattice systems: a time-dependent superoperator renormalization algorithm. *Phys. Rev. Lett.* **2004**, *93*, 207205.
(20) Feiguin, A. E.; White, S. R. Finite-temperature density matrix renormalization using an enlarged Hilbert space. *Phys. Rev. B: Condens. Matter Mater. Phys.* **2005**, *72*, 220401.
(21) Barthel, T.; Schollwöck, U.; White, S. R. Spectral functions in one-dimensional quantum systems at finite temperature using the density matrix renormalization group. *Phys. Rev. B: Condens. Matter Mater. Phys.* **2009**, *79*, 245101.
(22) Gobert, D.; Kollath, C.; Schollwöck, U.; Schütz, G. Real-time dynamics in spin-1 2 chains with adaptive time-dependent density matrix renormalization group. *Phys. Rev. E* **2005**, *71*, 036102.
(23) Kloss, B.; Lev, Y. B.; Reichman, D. Time-dependent variational principle in matrix-product state manifolds: Pitfalls and potential. *Phys. Rev. B: Condens. Matter Mater. Phys.* **2018**, *97*, 024307.
(24) Hallberg, K. A. Density-matrix algorithm for the calculation of dynamical properties of low-dimensional systems. *Phys. Rev. B: Condens. Matter Mater. Phys.* **1995**, *52*, R9827.
(25) Ramasesha, S.; Pati, S. K.; Krishnamurthy, H.; Shuai, Z.; Brédas, J. Low-lying electronic excitations and nonlinear optic properties of polymers via symmetrized Density Matrix Renormalization Group Method. *Synth. Met.* **1997**, *85*, 1019−1022.
(26) Shuai, Z.; Brédas, J.; Saxena, A.; Bishop, A. Linear and nonlinear optical response of polyenes: a density matrix renormalization group study. *J. Chem. Phys.* **1998**, *109*, 2549−2555.
(27) Kühner, T. D.; White, S. R. Dynamical correlation functions using the density matrix renormalization group. *Phys. Rev. B: Condens. Matter Mater. Phys.* **1999**, *60*, 335.
(28) Jeckelmann, E. Dynamical density-matrix renormalization-group method. *Phys. Rev. B: Condens. Matter Mater. Phys.* **2002**, *66*, 045114.
(29) Dorando, J. J.; Hachmann, J.; Chan, G. K.-L. Analytic response theory for the density matrix renormalization group. *J. Chem. Phys.* **2009**, *130*, 184111.
(30) Holzner, A.; Weichselbaum, A.; McCulloch, I. P.; Schollwöck, U.; von Delft, J. Chebyshev matrix product state approach for spectral functions. *Phys. Rev. B: Condens. Matter Mater. Phys.* **2011**, *83*, 195115.
(31) Nakatani, N.; Wouters, S.; Van Neck, D.; Chan, G. K.-L. Linear response theory for the density matrix renormalization group: Efficient algorithms for strongly correlated excited states. *J. Chem. Phys.* **2014**, *140*, 024108.
(32) Dargel, P.; Wöllert, A.; Honecker, A.; McCulloch, I.; Schollwöck, U.; Pruschke, T. Lanczos algorithm with matrix product states for dynamical correlation functions. *Phys. Rev. B: Condens. Matter Mater. Phys.* **2012**, *85*, 205119.
(33) Xie, H.; Huang, R.; Han, X.; Yan, X.; Zhao, H.; Xie, Z.; Liao, H.; Xiang, T. Reorthonormalization of Chebyshev matrix product states for dynamical correlation functions. *Phys. Rev. B: Condens. Matter Mater. Phys.* **2018**, *97*, 075111.
(34) Kokalj, J.; Prelovšek, P. Finite-temperature dynamics with the density-matrix renormalization group method. *Phys. Rev. B: Condens. Matter Mater. Phys.* **2009**, *80*, 205117.
(35) Tiegel, A. C.; Manmana, S. R.; Pruschke, T.; Honecker, A. Matrix product state formulation of frequency-space dynamics at finite temperatures. *Phys. Rev. B: Condens. Matter Mater. Phys.* **2014**, *90*, 060406.
(36) Schollwöck, U. The density-matrix renormalization group in the age of matrix product states. *Ann. Phys.* **2011**, *326*, 96−192.
(37) Chan, G. K.-L.; Keselman, A.; Nakatani, N.; Li, Z.; White, S. R. Matrix product operators, matrix product states, and ab initio density matrix renormalization group algorithms. *J. Chem. Phys.* **2016**, *145*, 014102.
(38) Li, W.; Ren, J.; Shuai, Z. Numerical assessment for accuracy and GPU acceleration of TD-DMRG time evolution schemes. *J. Chem. Phys.* **2020**, *152*, 024127.
(39) Spano, F. C. Temperature dependent exciton emission from herringbone aggregates of conjugated oligomers. *J. Chem. Phys.* **2004**, *120*, 7643−7658.
(40) Spano, F. C. The spectral signatures of Frenkel polarons in H- and J-aggregates. *Acc. Chem. Res.* **2010**, *43*, 429−439.
(41) Spano, F. C.; Yamagata, H. Vibronic coupling in J-aggregates and beyond: a direct means of determining the exciton coherence length from the photoluminescence spectrum. *J. Phys. Chem. B* **2011**, *115*, 5133−5143.
(42) Li, W.; Peng, Q.; Ma, H.; Wen, J.; Ma, J.; Peteanu, L. A.; Shuai, Z. Theoretical Investigations on the Roles of Intramolecular Structure Distortion versus Irregular Intermolecular Packing in Optical Spectra of 6T Nanoparticles. *Chem. Mater.* **2017**, *29*, 2513−2520.
(43) Ghosh, R.; Chew, A. R.; Onorato, J.; Pakhnyuk, V.; Luscombe, C. K.; Salleo, A.; Spano, F. C. Spectral signatures and spatial coherence of bound and unbound polarons in p3ht films: Theory versus experiment. *J. Phys. Chem. C* **2018**, *122*, 18048−18060.
(44) Meier, T.; Zhao, Y.; Chernyak, V.; Mukamel, S. Polarons, localization, and excitonic coherence in superradiance of biological antenna complexes. *J. Chem. Phys.* **1997**, *107*, 3876−3893.
(45) Moix, J. M.; Zhao, Y.; Cao, J. Equilibrium-reduced density matrix formulation: Influence of noise, disorder, and temperature on localization in excitonic systems. *Phys. Rev. B: Condens. Matter Mater. Phys.* **2012**, *85*, 115412.
(46) Song, L.; Shi, Q. A new approach to calculate charge carrier transport mobility in organic molecular crystals from imaginary time path integral simulations. *J. Chem. Phys.* **2015**, *142*, 174103.
(47) Ambrosek, D.; Kohn, A.; Schulze, J.; Kühn, O. Quantum chemical parametrization and spectroscopic characterization of the frenkel exciton hamiltonian for a J-aggregate forming perylene bisimide dye. *J. Phys. Chem. A* **2012**, *116*, 11451−11458.
(48) Schröter, M.; Ivanov, S.; Schulze, J.; Polyutov, S.; Yan, Y.; Pullerits, T.; Kühn, O. Exciton−vibrational coupling in the dynamics and spectroscopy of Frenkel excitons in molecular aggregates. *Phys. Rep.* **2015**, *567*, 1−78.
(49) Saad, Y. *Iterative Methods for Sparse Linear Systems*, 2nd ed.; Society for Industrial and Applied Mathematics: Philadelphia, 2003.

https://dx.doi.org/10.1021/acs.jpclett.0c00905
J. Phys. Chem. Lett. 2020, 11, 3761−3768

(50) Zhang, C.; Jeckelmann, E.; White, S. R. Dynamical properties of the one-dimensional Holstein model. *Phys. Rev. B: Condens. Matter Mater. Phys.* **1999**, *60*, 14092.

https://dx.doi.org/10.1021/acs.jpclett.0c00905
J. Phys. Chem. Lett. 2020, 11, 3761−3768